



Numerical modelling of particle entrainment in the wheel–rail interface

Sadaf Maramizonouz¹ · Sadegh Nadimi¹ · William A. Skipper² · Stephen R. Lewis³ · Roger Lewis²

Received: 13 January 2023 / Revised: 17 April 2023 / Accepted: 20 April 2023 / Published online: 17 May 2023
© The Author(s) 2023

Abstract

The process of applying sand particles to increase the traction between wheel and rail is reported to be less than 20% efficient. To better understand entrainment efficiency, the process is simulated using the Discrete Element Method. The simulation results are validated against full-scale experimental observations in terms of entrainment efficiency and particle velocity for ten case studies with different positioning of the sand nozzle. The numerical simulations confirm the experimental observations wherein the highest efficiency can be achieved when the sander is aimed at the wheel/rail nip. When aiming the sander at the wheel, the values of entrainment efficiency from simulations and experiments show some discrepancy which can be related to the numerical assumptions. Calculating coefficients of traction between the rail and wheel from the simulation data for the four cases of an un-sanded contact, and with the sander aimed at the rail, the nip, and the wheel (all with the same angle) show an increase in the coefficient of traction for all sanded cases compared to the un-sanded case.

Keywords Traction · Adhesion · Particles · Numerical analysis

1 Introduction

The traction or adhesion¹ between wheel and rail has been a significant area of research for many years with the aim being to improve railway transportation. This is due to the crucial role traction plays in train kinematics and performance, especially during acceleration and deceleration phases of the train dynamics [1–3]. Inadequate traction reduces train acceleration and can cause train delays. The loss of traction or its decrease to insufficient levels constitutes risks, safety issues, and ultimately may result in train collisions [4–6]. Low traction levels can occur when a layer of water, leaf contamination, oil, or other materials form on or bond to the

top surface of the rail. One method of increasing the traction between the wheel and the rail is utilising a train-borne device to apply sand particles to the wheel/rail interface in a stream of compressed air, which is called rail sanding [2, 5–7]. Figure 1a shows the schematic of a sander set-up.

During rail-sanding only < 20% of sand particles land on the desired area and act as a third body layer between the rail and wheel [1]. In other words, the majority of sand particles are expelled and wasted. This presents a potential to design and optimise sanding systems to increase the efficiency of sand application (entrainment efficiency) which is key to adjusting the rail-wheel traction levels and thus controlling the risks of railway transportation. It can also introduce a more sustainable approach to using sand considering its limited resources [2, 3, 5].

To optimise the sanding process, Lewis et al. [1] investigated the effects of sander nozzle positioning relative to the wheel and rail for ten case studies using a full-scale laboratory wheel–rail test rig. They calculated the entrainment efficiency for each case study by collecting the sand remaining on the rail after the wheel had passed and dividing its mass by the total mass of the sand exiting the sander. By comparing the entrainment efficiency results, they were able to propose optimised positions for the sander nozzle [1].

¹ In the railway industry “adhesion” or “adhesion coefficient” is defined as the amount of traction present when the wheel–rail contact enters partial slip. In this paper, the terms are used interchangeably.

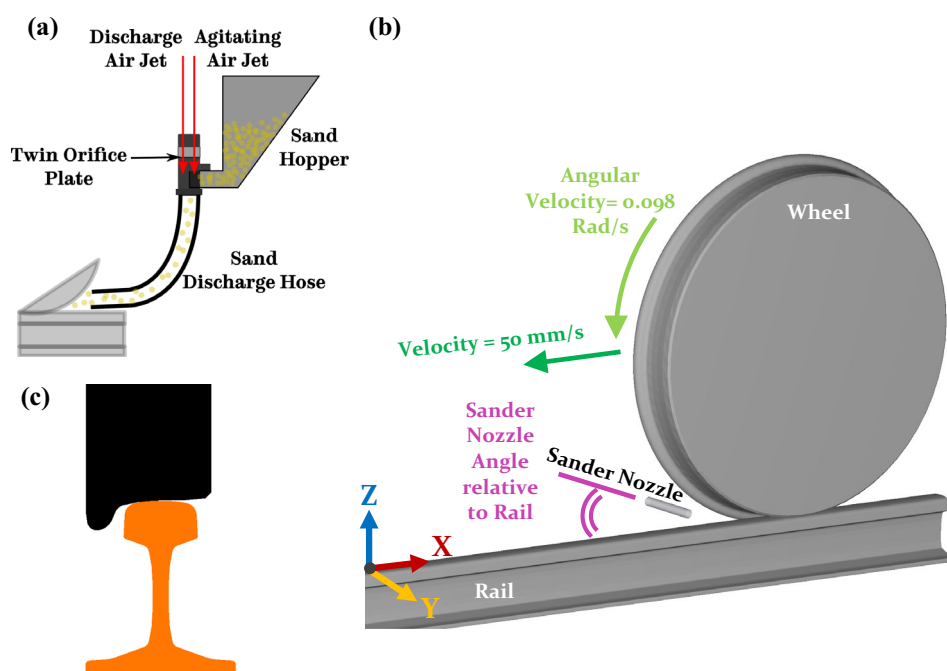
✉ Sadegh Nadimi
sadegh.nadimi-shahraki@ncl.ac.uk

¹ School of Engineering, Newcastle University, Newcastle upon Tyne NE1 7RU, UK

² Department of Mechanical Engineering, Leonardo Centre for Tribology, University of Sheffield, Sheffield S1 3JD, UK

³ Rail Technologies Department, British Steel, Scunthorpe Rail and Section Mill, Brigg Road, Scunthorpe DN16 1BP, UK

Fig. 1 **a** Schematic of a typical sander set-up, **b** geometry layout for the numerical model of one case study, and **c** closeup of the 60E1 rail and P8 wheel profile



The studies on physical interactions of wheel and rail and sometimes sand is largely limited to experimental observations and computational modelling. Experimental studies to investigate the effects of particle size on adhesion and wear have been performed through twin-disc experiments [2] and field tests [8]. Twin-disc experiments have also been conducted to study the adhesion, wear and damage of wheel and rail in different conditions [9, 10]. The effects of different materials used for rail-sanding on the performance of track circuits have been investigated as well [11]. Experimental investigation in a controlled environment offers accurate observations, however they are expensive and less accessible for a wider community and investigation.

Computational modelling of wheel–rail interaction and rail-sanding are typically performed using finite element method (FEM) such as the study by Duan [12]. However, the sanding process is multiscale and multiphase for which FEM is not the most practical modelling tool especially in addressing the dynamics of a third body layer, i.e., sand particles. As an alternative to FEM modelling, the discrete element method (DEM) can be adopted such as the study by Descartes et al. [13] where DEM has been used to address the wheel–rail isolation issue. Another example is the modelling method proposed by Gautam and Green [14] where they coupled their DEM model to computational fluid dynamics (CFD) to present a high-fidelity computational simulation. CFD-DEM coupling can drastically increase computational time and cost which may be a reason why Gautam and Green [14] scaled down the geometry of their setup compared to the actual rail-sanding systems. They have also introduced a gap in the wheel–rail interface between the wheel and the rail which

although simplifies the calculation of entrainment efficiency, is not a realistic assumption and prevents the investigation of wheel–rail traction.

In this study, DEM modelling is employed to directly simulate the interactions between thousands of particles in a full-scale rail-sanding setup. The aim is to investigate the entrainment efficiency of sand particles through DEM simulations and validate the results against the data presented by Lewis et al. [1] for various positions of the sander nozzle. Sand particle velocities, coefficient of traction and spread angle of the sand particles are also investigated.

2 Methodology

2.1 Discrete element method

Particle mechanics during the rail sanding process are investigated with the assumption of the particles being rigid discrete objects. These discrete particles can then be individually tracked by solving Newton's and Euler's laws of motion [15]. The dynamics of an individual particle can be modelled through the governing equations of its translational and rotational motion, presented as follows:

$$m_i \frac{d\mathbf{v}_i}{dt} = \sum \mathbf{F}_{C_i} + m_i \mathbf{g} \quad (1)$$

$$d(\mathbf{I}_i \cdot \boldsymbol{\omega}_i)/dt = \sum \mathbf{M}_{C_i} \quad (2)$$

Table 1 Material characteristics and dynamic properties of simulation components [1, 6]

Simulation Component	Density (kg/m ³)	Young's Modulus (GPa)	Poisson's ratio	Translational Velocity (m/s)	Rotational Velocity (rad/s)	Coefficient of Restitution
Sand	2650	70	0.25	5.0	–	0.5
Sander Nozzle	7600	240	0.3	0	–	–
Wheel	7600	240	0.3	0	0.098	–
Rail	7600	240	0.3	0.05	–	–

where m_i is the particle's mass, v_i is the particle's translational velocity, t is time, F_{Ci} is the contact force between each particle and its neighbouring particles and walls, g is the gravitational acceleration, I_i is the particle's moment of inertia, ω_i is the particle's rotational velocity, and M_{Ci} is the contact torque which is equal to $R_i \times F_{Ci}$ the cross product of the particle's radius (R_i) and the contact force [15].

The interparticle and particle–wall interactions are modelled using a Hertz-Mindlin contact model which is an elastic contact force discussed in detail in reference [15]. The Hertz-Mindlin contact model although may not represent the contact dynamics of actual sand grains, can be considered accurate enough for the application presented in the current research. However, choosing a more accurate contact model can result to better prediction of tangential forces. For example, Nadimi et al. [16] utilised a combination of Boundary Element Method (BEM) and DEM to develop a new contact model which can represent the effect of asperities in the contact. More information on available contact models for implementing the effects surface roughness in DEM modelling can be found in Nadimi et al. [17].

2.2 Numerical model

The numerical set-up for DEM modelling of rail-sanding is developed based on the full-scale wheel–rail rig at the Leonardo Centre for Tribology—The University of Sheffield [1]. The geometries of the wheel, rail, and sander are defined as a wheel with a diameter of ~ 1016 mm and a P8 profile, a 60E1 rail with a width of ~ 70 mm and a length of nearly three times of the wheel diameter, and a cylindrical sander nozzle with length and diameter of 150 mm and 25 mm (according to the use of a hose with the same dimensions as the sander by Lewis et al. [1]), respectively. The wheel and the rail are modelled as solid bodies while the sander nozzle is modelled as a hollow cylindrical tube. Particles are represented as a dilute suspension of spherical particles with 2 mm diameter, with a density of 2650 kg/m³, a Young's modulus of 70 GPa, a Poisson's ratio of 0.25, and a coefficient of restitution of 0.5 on steel [6]. Figure 1b shows the geometry layout of the numerical model and Fig. 1c presents a closeup of the 60E1 rail and P8 wheel profile.

The wheel's translational and rotational velocities are set to 0.05 m/s, and 0.098 rad/s, respectively. The mass flow rate of the sand exiting the sander is 0.03 kg/s which makes the particles' initial velocities 5 m/s in the direction of sander nozzle. Table 1 presents the material characteristics and dynamic properties of simulation components. The coefficient of restitution between sand particles and steel is a physical property and is implemented in the DEM modelling in order to damp the bouncing of the particles after their interaction with the geometries [18].

Ten case studies, presented in Table 2, are investigated, changing the sander's position and angle relative to the rail surface based on the work of Lewis et al. [1].

DEM simulations are performed using Altair EDEM software (version 7.1.0) and the time step is set to 1e⁻⁶. The results produced through simulations in this study are compared to the data presented by Lewis et al. [1].

3 Results and discussions

3.1 Entrainment Efficiency for Sand Particles

Snapshots of sand entrainment obtained from (1) DEM simulations, and (2) experiments by Lewis et al. [1] for three case studies of sander position are presented in Fig. 2: nozzle (a) aimed at the rail with a 20° angle, (b) aimed at the nip with a 20° angle, and (c) aimed at the wheel with a 20° angle.

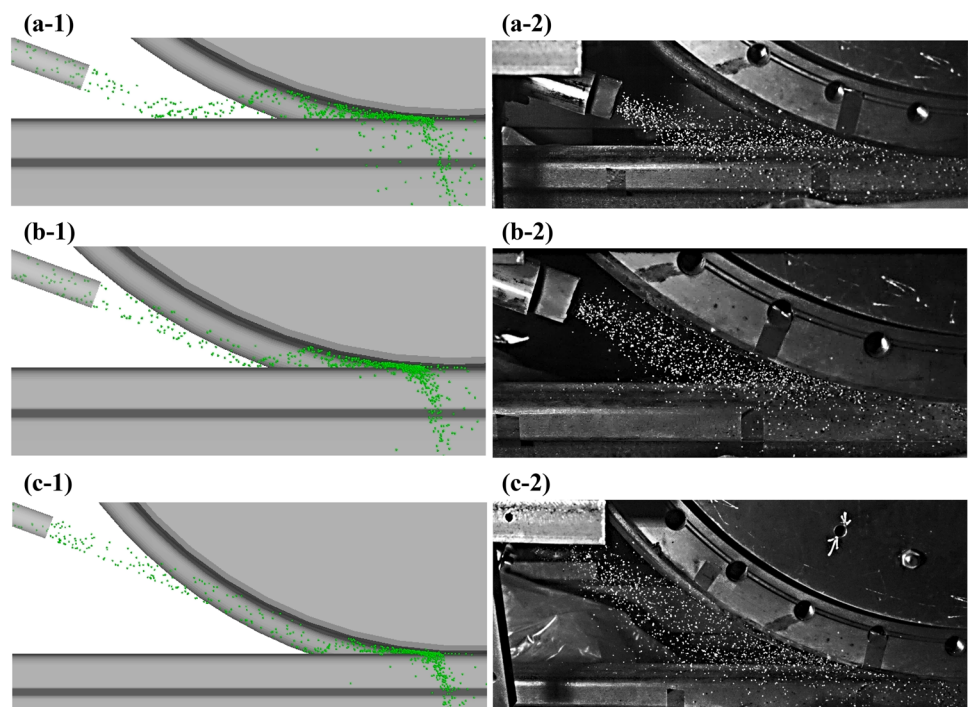
The entrainment efficiency of the sand particles can be described as the ratio of the mass of sand that passes into the nip between the rail and wheel to the mass of sand that leaves the sander nozzle. The entrainment efficiencies for all ten case studies obtained from the simulations are compared to the data reported for each case study by Lewis et al. [1] and are presented in Fig. 3.

In the experimental work of Lewis et al. [1], the sand that passed through the contact and remained on the surface of the rail at the end of the test is collected and its mass is measured. The entrainment efficiency can then be estimated by dividing the measured mass by the mass of the sand used during the experiment [1].

Table 2 Sander set-up geometry (based on the work of Lewis et al. [1])

Sander aimed at	Sander aimed at a point of the rail from centre of contact (mm)	Sander distance from contact patch (mm)	Sander height above rail (mm)	Sande angle to rail (°)
Rail	200	350	20	15
	200	348	33	20
	200	344	45	25
	200	340	58	30
Nip	100	330	20	10
	100	327	40	15
	100	323	60	20
Wheel	300	440	156	5
	300	451	104	10
	300	448	131	20

Fig. 2 Particle entrainment for three case studies of the sander **a** aimed at the rail with a 20° angle, **b** aimed at the nip with a 20° angle, and **c** aimed at the wheel with a 20° angle relative to the rail surface obtained from (1) current simulations and (2) experiments presented by Lewis et al. [1]



In order to calculate the entrainment efficiency for the DEM simulations, a rectangular geometry bin needs to be defined in the simulation software to count the number of particles passing through the contact. Here, three geometry bins with different dimensions of 35 mm × 20 mm × 20 mm (Fig. 3(a)) for the small bin, 40 mm × 20 mm × 20 mm (Fig. 3b) for the medium bin, and 45 mm × 20 mm × 20 mm (Fig. 3c) for the large bin, all with their centres located at the point of wheel and rail contact are considered (i.e. $x = 27$ mm, $y = 0$ mm, and $z = 10$ mm). Defining different sizes and positions for the geometry box affects the value of the entrainment efficiency, but conserves the trends as can be seen in Fig. 3.

When aiming the sander nozzle at the rail and at the nip, the values of entrainment efficiency from simulations and experiments are comparable. However, aiming the sander at the wheel results in a large difference between the values of entrainment efficiency from simulations and experiments. This can be attributed to the angle of spread when sand particles exit the nozzle.

In the experiment, the sand particles show a larger spread angle as they are sprayed out than in the numerical simulation as depicted in Fig. 2. The spread angle is larger for the cases where the sander nozzle is aimed at the wheel (Fig. 2c) compared to the other cases (Fig. 2a and Fig. 2b) due to the larger distance between the sander nozzle aimed at the wheel and the

Fig. 3 Entrainment efficiency for all ten case studies obtained from current simulations (depicted by green) for **a** geometry bin 1, **b** geometry bin 2, **c** geometry bin 3 compared to the data presented by Lewis et al. [1] (depicted by blue), and **d** comparison of the values of the entrainment efficiency for the three different sizes of the geometry bins

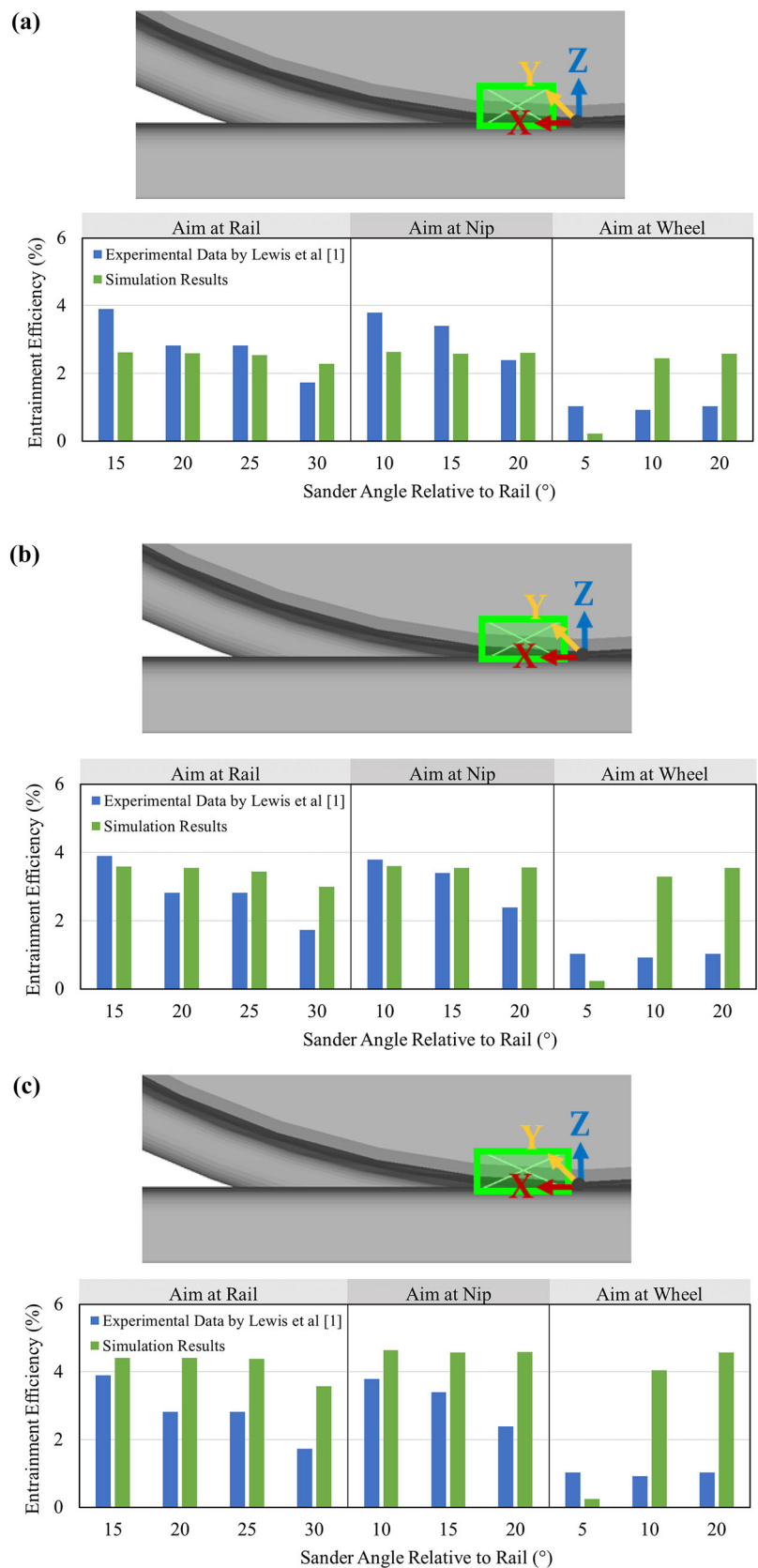
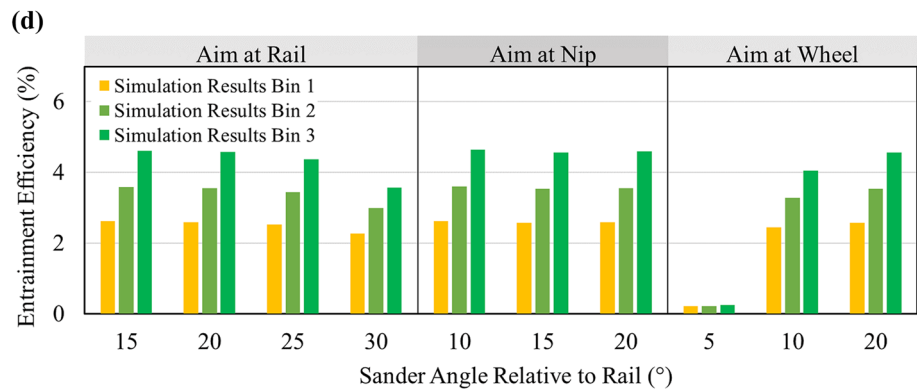


Fig. 3 continued



the wheel/rail nip. This could be the reason why the values of entrainment efficiency show the most difference between the experiments and simulations when the sander nozzle is aimed at the wheel. It is also worth noting that aiming the sander at the wheel does not represent a real positioning condition for the sander used for rail-sanding practice.

Figure 3d compares the values of the entrainment efficiency for the three different sizes of the geometry bins.

3.2 Velocity of the sand particles

To extract the particle velocities, the high-speed videos of all ten experimental case studies recorded by Lewis et al. [1] have been reprocessed using the digital Particle Image Velocimetry (PIV) tool in MATLAB called PIVlab (version 2.57) [19–21]. To use PIVlab, the high-speed videos are loaded into the toolbox and presented frame-by-frame. Here the first ~ 500 frames of each video are removed due to the method of performing the experiments which results in partially blocking the camera lens for a few seconds. Then the region of interest is defined as the region in which only the particles exist, move and interact in order to limit the area being processed and to eliminate other moving parts such as the wheel and the rail. After that the images are pre-processed to distinguish between the moving particles and the background. The toolbox utilises a Fast Fourier Transform (FFT) window deformation method to analyse all the frames and extract the velocity data. The data can be calibrated using a known distance from the experimental set-up in the video (here the sander diameter of 25 mm) and the time step between every two frames (the videos are captured at 750 fps which results in a time step of 1.333 ms). The extracted PIV data (dashed line) are compared to the simulation results (solid line) in Fig. 4 which shows good agreement between the simulation and experimental results.

The initial discrepancy in Fig. 4 is due to the removal of the ~ 500 frames from the beginning of each experimental video. From ~ 0.4 s onwards, it can be seen that the values for the sand particles' velocities compare very well for the

simulations and experiments for most of the cases. Particles exit the sander nozzle with an initial velocity of 5 m/s in the direction of the sander nozzle. Then they start to descend from the height of the sander nozzle towards the surface of the rail under the effects of gravity while their velocity decreases during the first ~ 0.5 s of the simulation. After that, they maintain a relatively constant velocity which is comparable to the experimental data extracted from the high-speed videos.

The highest percentage of difference between the simulation and experimental results is ~ 40% which belongs to the two cases, where the sander nozzle was aimed at the wheel at 5° (Fig. 4h) and 10° (Fig. 4i) angles relative to the rail surface.

3.3 Investigating the coefficient of traction

The Coefficient of Traction (CoT) between the rail and the wheel is defined as the ratio of the shear force to the normal force experienced by the rail. In typical DEM simulations, only particle-to-particle and particle-to-geometry interactions can be studied and the geometry-to-geometry interactions (in this case between rail and wheel) do not influence the simulation results. One approach to circumvent this shortcoming is to represent at least one of the solid geometries as a cluster of bonded fragments. This approach makes the investigation of the interactions between the discrete fragments and the solid geometries possible.

In this research, the rail is chosen as the only geometry to be represented as a cluster of bonded, tightly packed spherical steel fragments. The cluster of spherical steel fragments is generated inside a physical but hollow geometry in the shape of the rail. The radius of these spherical fragments ranges from 3 to 7 mm and they are bonded using solid bonds with a 3 mm diameter (for more information on bond characteristics in DEM simulations please refer to [22]). The cluster representation of the rail is shown in Fig. 5a.

The advantage of considering the rail as a physical but hollow geometry filled with spherical fragments is that the third-body sand particles will remain on the top surface of the

Fig. 4 Particle velocity obtained from simulation (lighter colour dashed line) and extracted from experimental videos by digital PIV (darker colour solid line) for case studies of the sander nozzle aimed at the rail with a **a** 15° angle, **b** 20° angle, **c** 25° angle, and **d** 30° angle, the sander aimed at the nip with a **e** 10° angle, **f** 15° angle, and **g** 20° angle, and the sander aimed at the wheel with a **h** 5° angle, **i** 10° angle, and **j** 20° angle relative to the rail surface

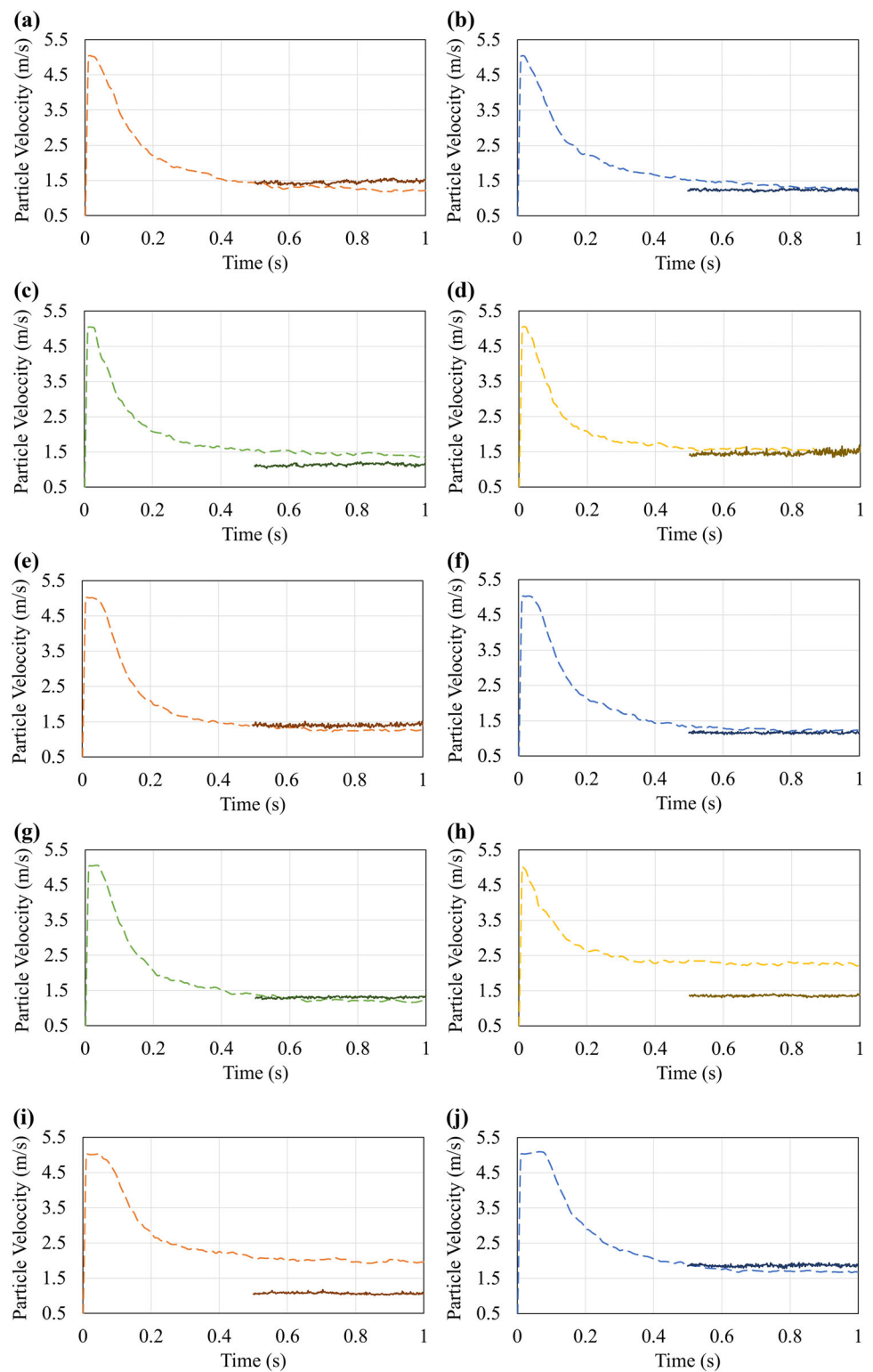
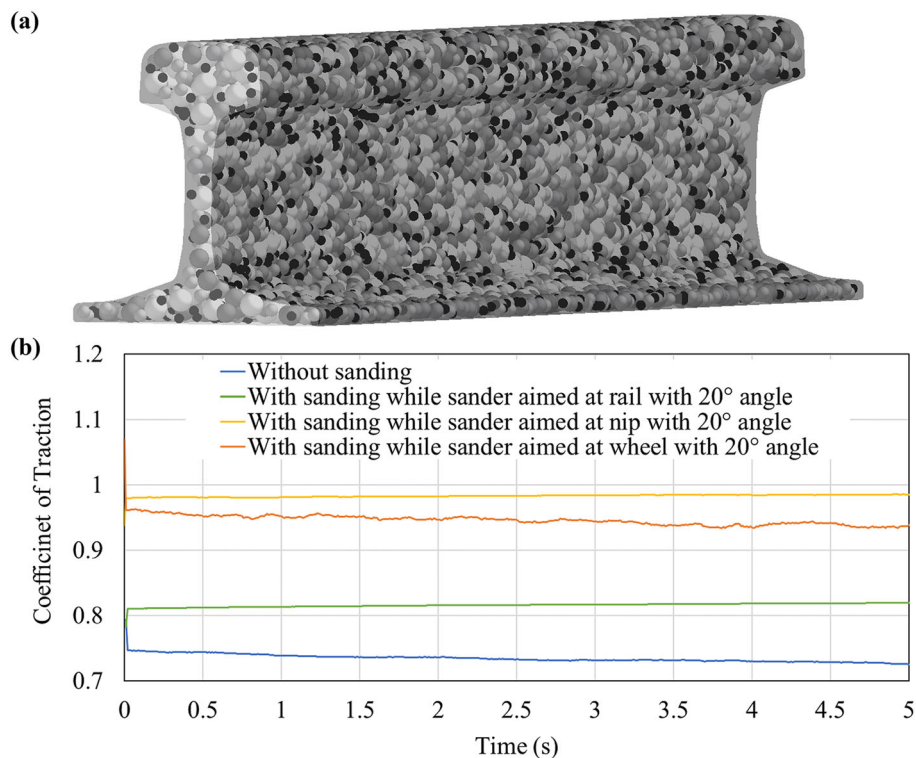


Fig. 5 a The representation of the rail as a cluster of bonded, tightly packed spherical steel fragments with radiuses ranging from 3 to 7 mm, and **b** Coefficient of traction for the case without sanding (blue), and with sander aimed at the rail with a 20° angle (green), aimed at the nip with a 20° angle (yellow), and aimed at the wheel with a 20° angle (orange) relative to the rail surface obtained from current simulations



rail geometry which prevents them from directly interacting with and hiding inside the asperities between the spherical steel fragments. It is also worth mentioning that although replacing geometry with its cluster sphere representation may create an artificial roughness on the surface of the geometry, this artificial roughness will be similar for all the numerical simulations and thus the stand-alone effects of the presence of third-body in wheel–rail contact can be modelled.

With this approach, it would be possible to study the interactions between the wheel and the spherical fragments composing the rail and to estimate the value of CoT. To calculate the CoT at each timestep, the values of the tangential and normal stresses are averaged on all the elements composing the rail. The ratio of the average tangential stress to the average normal stress is calculated as the coefficient of traction, and is presented in Fig. 5b.

It can be seen from the simulation data that adding the sand particles between the train wheel and rail increases the CoT by $\sim 9.7\%$ when the sander nozzle is aimed at the rail at a 20° angle, by $\sim 25.1\%$ when the sander nozzle is aimed at the nip with a 20° angle, and by $\sim 22.3\%$ when the sander nozzle is aimed at the wheel with a 20° angle relative to the rail surface.

The coefficient of traction (CoT) can be affected by both the number of particles in the wheel–rail interface (i.e. the entrainment efficiency which is calculated for the total duration of the simulation as the ratio of the average number of

particles in the wheel–rail interface to the total number of particles) and the rate of sanding (i.e. the particle velocity which is calculated as the average particle velocity at each time step).

The entrainment efficiency when the sander is aimed at the nip, rail, and wheel is 3.56%, 3.55%, and 3.54%, respectively and the particle velocity is 1.30 m/s, 1.24 m/s, and 1.85 m/s, respectively. When the nozzle is aimed exactly at the wheel–rail interface which is the nip, a higher number of particles are present at the wheel–rail interface at each time step. So, the CoT is the highest. When the nozzle is aimed elsewhere, more particles bounce around and do not enter the wheel–rail interface at any given time step. Comparing the two cases of the sander aimed at the rail, and the wheel, the sanding rate is higher for the latter. So, the CoT is higher when the sander is aimed at the wheel.

The values of CoT were not reported in the experimental work of Lewis et al. [1], however, in another research [23] they investigated the wheel–rail adhesion and reported the values of CoT between 0.3 and 0.6. The present simulation may not reflect the exact values of CoT but presented reasonable trends for the four different cases. Finally, the study of the coefficient of traction between the wheel and the clump representation of the rail and can benefit from further investigations.

3.4 Introducing particle spread during rail sanding

In full-scale experiments, the sand particles used for rail-sanding exit the sander nozzle with a spread angle as depicted in Fig. 2(a-2), (b-2), and (c-2). This can be a result of various factors which have not been considered in simulations reported in Sect. 3.1, such as the interaction and dynamics of sand particles inside the hopper and as they move through the sander hose before exiting the sander. To model the spread of sand particles, the spread angle can be introduced and added to the simulations as an input parameter. This can be done through Altair EDEM’s user interface and by defining a spray of particles with both a velocity and a spread angle instead of setting only a fixed initial velocity for the sand particles. Figure 6a–c show the simulation results of the sander nozzle aimed at the rail, nip, and wheel with a 20° angle, respectively, and with a particle spread angle of 60°. Qualitatively, these results compare better with the experimental results of Fig. 2. However, the entrainment efficiency for the three cases of the sander aimed at the rail, the nip, and the wheel with a 20° angle and with a particle spread angle of 60° (Fig. 6d) which is calculated using the medium bin is only scaled down and the trend is as previously reported in Fig. 3.

Adding the particles’ spread angle as an input parameter to the DEM simulations results in the values of the entrainment efficiency to approach the experimental values when spread angle is large Fig. 6d. The reason why adding the particle spread angle does not significantly improve the entrainment efficiency results for the other two cases of aiming the sander nozzle at rail and nip (Fig. 6a, b) is that here a fixed value of 60° for the particle spread angle is used for all three cases which close to the experimental particle spread angle for the case of aiming the sander nozzle at wheel with a 20° angle thus bringing the entrainment efficiency closer to the experimental values. While it is significantly larger compared to the experimental spread angle observed for the other two cases of aiming the sander nozzle at rail and nip with a 20° angle thus resulting in lower entrainment efficiency values for simulations compared to experiments.

4 Conclusions

In this research, DEM simulation of the rail-sanding application for ten case studies with different positioning of the sander nozzle was performed and the simulation results were validated against full-scale experimental data. The particle entrainment efficiency and particle velocity obtained from the simulation were compared to the data extracted from experimental videos using digital PIV. The values of entrainment efficiency calculated from the simulations are affected by the size and position of the geometry box, but the trends

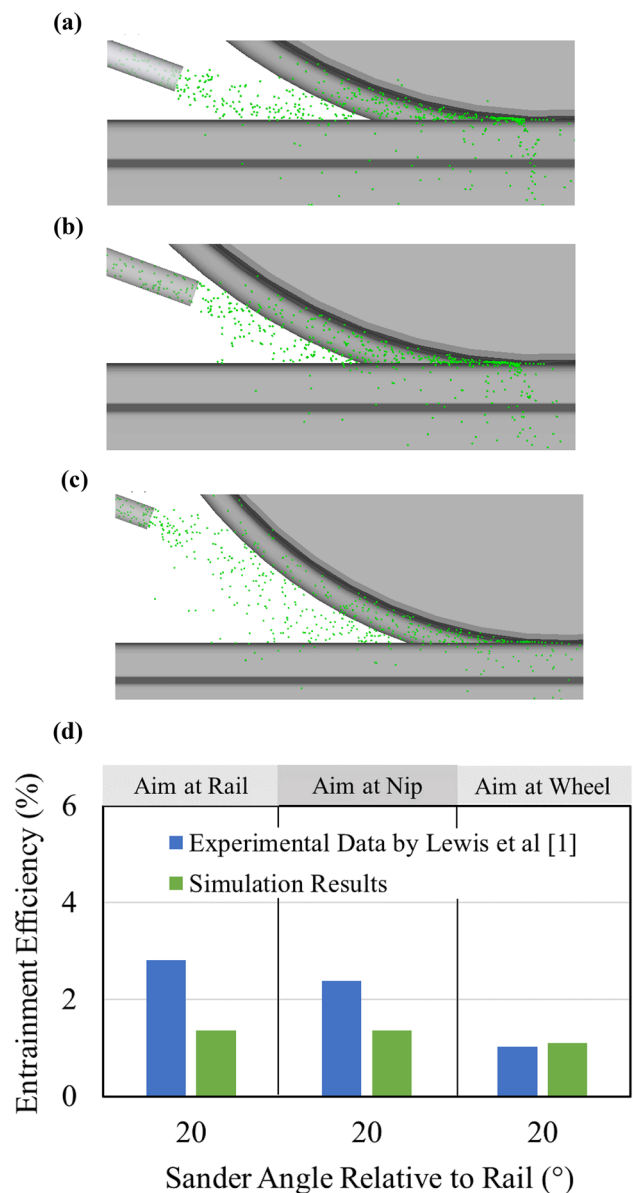


Fig. 6 Particle entrainment for three case studies of the sander **a** aimed at the rail with a 20° angle, **b** aimed at the nip with a 20° angle, and **(c)** aimed at the wheel with a 20° angle relative to the rail surface obtained from current simulations with a sand spray with a 60° spread angle and **d** Entrainment efficiency for the three case studies above, obtained from current simulations (depicted by green) for compared to the data presented by Lewis et al. [1] (depicted by blue)

remain the same. For seven of the ten cases, when the sander was aimed at rail and nip, the values of entrainment efficiency from simulations and experiments compare very well. But for the three cases when the sander was aimed at the wheel, the difference between the values of entrainment efficiency from simulations and experiments was larger. To investigate the reason behind this difference, the spread angle of the sand particles as they exit the sander nozzle was modelled by introducing the spread angle as an input parameter to the

simulations which produced lower entrainment efficiency of the sand particles compared to the cases without the spread which were less accurate for the cases of the sander aimed at rail and nip. This will need further investigations and is an area for the future works of this research. The sand particle velocities obtained from simulations and experiments compared well for eight of the ten cases. For the other two cases, with the sander aimed at the wheel with 5° and 10° angles, a difference of $\sim 40\%$ was observed. The coefficient of traction between the train wheel and rail was also investigated for the cases of an un-sanded contact, and with the sander aimed at the rail, the wheel/rail nip, and the wheel (all with a 20° angle) which showed an increase in CoT by $\sim 9.7\%$, $\sim 25.1\%$, and $\sim 22.3\%$ for each respective sanded case compared to the un-sanded case. Overall, as the sander nozzle is aimed closer to the wheel–rail interface (the nip), a higher number of sand particles land exactly at the wheel–rail interface. This will increase both entrainment efficiency and coefficient of traction. The simulation results presented here compared very well and were validated against experimental data. This is an important step towards developing a predictive model of rail sanding which can be an essential tool to avoid expensive testing and can be more widely available to system designers and operators. In the next steps, the effects of different particle properties and the existence of moisture content between particles, different train velocities, and the presence of water and leaf contamination as well as crosswinds on the entrainment efficiency and CoT through computational simulations will be investigated.

Acknowledgements This work was funded by the UK Engineering and Physical Sciences Research Council (EPSRC) grant No. EP/V053655/1 RAILSANDING—Modelling Particle Behaviour in the wheel–Rail Interface. The authors would like to thank the UK Rail Safety and Standards Board (RSSB) for supporting the full-scale experiments (T797 project) reported here.

Declarations

Conflict of interest The authors declare that they have no known competing financial interests or personal relationships that could have appeared to influence the work reported in this paper.

Open Access This article is licensed under a Creative Commons Attribution 4.0 International License, which permits use, sharing, adaptation, distribution and reproduction in any medium or format, as long as you give appropriate credit to the original author(s) and the source, provide a link to the Creative Commons licence, and indicate if changes were made. The images or other third party material in this article are included in the article's Creative Commons licence, unless indicated otherwise in a credit line to the material. If material is not included in the article's Creative Commons licence and your intended use is not permitted by statutory regulation or exceeds the permitted use, you will need to obtain permission directly from the copyright holder. To view a copy of this licence, visit <http://creativecommons.org/licenses/by/4.0/>.

References

- Lewis S, Riley S, Fletcher D, Lewis R (2018) Optimisation of a railway sanding system for optimal grain entrainment into the wheel–rail contact. *Proc Inst Mech Eng Part F J Rail Rapid Transit* 232(1):43–62
- Arias-Cuevas O, Li Z, Lewis R (2011) A laboratory investigation on the influence of the particle size and slip during sanding on the adhesion and wear in the wheel–rail contact. *Wear* 271(1–2):14–24. <https://doi.org/10.1016/j.wear.2010.10.050>
- Skipper W, Chalisey A, Lewis R (2020) A review of railway sanding system research: wheel/rail isolation, damage, and particle application. *Proc Inst Mech Eng Part F J Rail Rapid Transit* 234(6):567–583
- GMRT2461 (2018) Sanding Equipment (Issue 3), R. S. a. S. Board
- Skipper WA, Chalisey A, Lewis R (2018) A review of railway sanding system research: adhesion restoration and leaf layer removal. *Tribol Mater Surf Interfac* 12(4):237–251
- Skipper W, Nadimi S, Chalisey A, Lewis R (2019) Particle characterisation of rail sands for understanding tribological behaviour. *Wear* 432:202960
- Cooper P (1972) An investigation into the relationship between the particle size and the frictional performance of sand (IM-ADH-011), British Rail Research. [Online]. Available: <https://www.sparkrail.org/Lists/Records/DispForm.aspx?ID=10483>
- Arias-Cuevas O, Li Z (2011) Field investigations into the performance of magnetic track brakes of an electrical multiple unit against slippery tracks. Part 1: adhesion improvement. *Proc Inst Mech Eng Part F J Rail Rapid Transit* 225(6):613–636
- Lewis R, Dwyer-Joyce R (2006) Wear at the wheel/rail interface when sanding is used to increase adhesion. *Proc Inst Mech Eng Part F J Rail Rapid Transit* 220(1):29–41
- Wang C et al (2021) Adhesion and damage characteristics of wheel/rail using different mineral particles as adhesion enhancers. *Wear* 477:203796
- Skipper W, Nadimi S, Lewis R (2021) Sand consist changes for improved track circuit performance (COF-UOS-03)
- Duan F (2015) Numerical tribology of the wheel–rail contact: application to corrugation defect. *INSA de Lyon*
- Descartes S et al (2008) A new mechanical–electrical approach to the wheel–rail contact. *Wear* 265(9–10):1408–1416
- Gautam A, Green SI (2021) Computational fluid dynamics—discrete element method simulation of locomotive sanders. *Proc Inst Mech Eng Part F J Rail and Rapid Transit* 235(1):12–21
- Thornton C (2015) Granular dynamics, contact mechanics and particle system simulations. A DEM study. *Particle Technology Series*, vol 24
- Nadimi S, Ghanbarzadeh A, Neville A, Ghadiri M (2020) effect of particle roughness on the bulk deformation using coupled boundary element and discrete element methods. *Comput Part Mech* 7(3):603–613. <https://doi.org/10.1007/s40571-019-00288-3>
- Nadimi S, Angelidakis V, Otsubo M, Ghanbarzadeh A (2022) How can the effect of particle surface roughness on the contact area be predicted? *Comput Geotech* 150:104890. <https://doi.org/10.1016/j.compgeo.2022.104890>
- Tsuji Y, Tanaka T, Ishida T (1992) Lagrangian numerical simulation of plug flow of cohesionless particles in a horizontal pipe. *Powder Technol* 71(3):239–250. [https://doi.org/10.1016/0032-5910\(92\)88030-L](https://doi.org/10.1016/0032-5910(92)88030-L)
- Thielicke W (2014) The flapping flight of birds. University of Groningen, Diss
- Thielicke W, Stamhuis E (2014) PIVlab—towards user-friendly, affordable and accurate digital particle image velocimetry in MATLAB J Open Res Softw. 2(1)

21. Thielicke W, Sonntag R (2021) Particle image velocimetry for MATLAB: accuracy and enhanced algorithms in PIVlab. *J Open Res Softw* 9(1)
22. Potyondy DO, Cundall PA (2004) A bonded-particle model for rock. *Int J Rock Mech Min Sci* 41(8):1329–1364. <https://doi.org/10.1016/j.ijmms.2004.09.011>
23. Lewis S, Riley S, Fletcher D, Lewis R (2017) Optimisation of a railway sanding system: adhesion tests. *Int J Railw Technol* 6(2):87–98

Publisher's Note Springer Nature remains neutral with regard to jurisdictional claims in published maps and institutional affiliations.